Tunable polarization mode conversion using thin-film lithium niobate ridge waveguide

GUANG YANG, [ID] **ALEXANDER V. SERGIENKO,** [ID] **AND ABDOULAYE NDAO**[*] [ID]

Department of Electrical and Computer Engineering & Photonics Center, Boston University, 8 Saint Mary's Street, Boston, MA 02215, USA
[*]*andao@bu.edu*

Abstract: Lithium niobate on insulator (LNOI) waveguides, as an emerging technology, have proven to offer a promising platform for integrated optics, due to their strong optical confinement comparable to silicon on insulator (SOI) waveguides, while possessing the versatile properties of lithium niobate, such as high electro-optic coefficients. In this paper, we show that mode hybridization, a phenomenon widely found in vertically asymmetric waveguides, can be efficiently modulated in an LNOI ridge waveguide by electro-optic effect, leading to a polarization mode converter with 97% efficiency. Moreover, the proposed device does not require tapering or periodic poling, thereby greatly simplifying the fabrication process. It can also be actively switched by external fields. Such a platform facilitates technological progress of photonics circuits and sensors.

1. Introduction

The pursuit of low-loss waveguides and on-chip optical components has been at the heart of the development of photonic integrated circuits. Lithium niobate offers an ideal platform due to its broad optical transparency, versatile nonlinear coefficients, and excellent electro-optic properties. Lithium niobate waveguides have been developed using conventional technologies such as proton-exchange [1] and titanium diffusion [2, 3]. However, such embedded waveguides have low index contrast and weak mode confinement, which hinders on-chip applications. Recently, the breakthrough in nanofabrication technologies has made low-loss waveguides possible in lithium niobate on insulator (LNOI) [4–6]. This new platform, featuring high index contrast and tight optical confinement [7], allows small footprints for on-chip components, as well as enables tightly bent structures [8, 9] and ring resonators [6, 10, 11]. Moreover, the compactness of LNOI waveguides greatly facilitates electro-optic modulation, since electrode pairs can be placed much closer, enhancing the efficiency of modulation. A variety of electro-optic applications in LNOI platforms have been demonstrated [12–15], among which a polarization converter, as a highly needed building block for photonic circuits, has been illustrated in [16]. This polarization converter is based on quasi-phase matching between two polarizations. While delivering great performance, this converter requires periodic poling. This increases the fabrication challenge, since periodic poling is typically done prior to waveguide fabrication to select the region with best poling quality [17].

Aside from the active approach using periodic poling, passive polarization converters in ridge waveguides can also be realized using mode hybridization phenomenon [18–21]. Modes that hybridize TE and TM components can arise from ridge waveguide geometries due to the breaking of symmetry along the vertical axis [18]. By tapering the waveguide around the hybrid regime, conversion between TE and TM modes can be achieved [19, 20]. Despite proposed methods, a device combining mode conversion and dynamic polarization modulation without tapering or periodic poling remains elusive. Here, we propose a novel mode conversion and polarization modulating scheme in LNOI ridge waveguides by introducing an electro-optically perturbed

index profile. We show the dynamic modulation of hybrid modes by external electric field and numerically demonstrate a polarization mode converter with 97% efficiency. This paves a new way for sophisticated photonic circuits and sensors that exploit the polarization degree of freedom [22, 23].

2. Waveguide design

The proposed device is illustrated in Fig. 1. The ridge waveguide is made in a 0.7 μm thick X-cut lithium niobate thin film with an etching depth of 0.6 μm. The lithium niobate thin film is bonded on a silicon dioxide layer to form the index contrast needed for optical guiding. The top cladding is air. The ordinary and extraordinary refractive indices of lithium niobate at the designed wavelength of 775 nm and room temperature (20 °C) are calculated to be 2.2586 and 2.1786, respectively, according to the Sellmeier equations in [24]. Mode conversion inside the waveguide is modulated by a transverse electric field in the x direction (see coordinates indicated in Fig. 1). The electric field is assumed to have a longitudinal gradient, leading to an index perturbation profile which also varies longitudinally, as will be elucidated later in the paper.
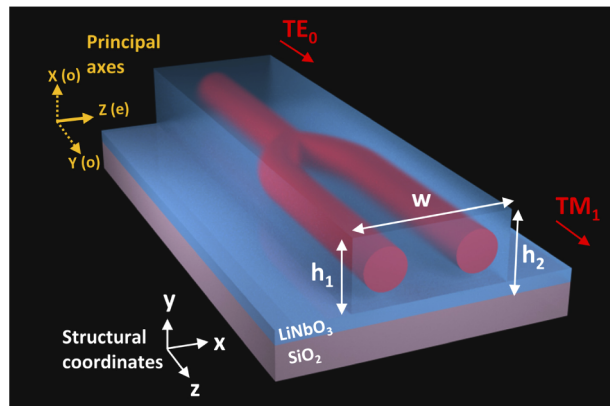

Fig. 1. A schematic of the proposed device. The lithium niobate layer thickness is h_2=0.7 μm. The considered etching depth is h_1=0.6 μm. The width w is a parameter under design and is chosen to be 1.1 μm in the final device. The principal axes (X, Y and Z) of the X-cut lithium niobate and the structural coordinates (x, y, and z) are indicated. The red beam depicts the mode with evolving shape along propagation.

To design such a device, we first consider the waveguide in a 2D cross section without perturbing the refractive index. In our study, the etching depth is fixed to at h_1=0.6 μm, and the waveguide width w is swept as the parameter under design to obtain mode hybridization. A fully vectorial finite difference mode solver (Lumerical MODE) is used for our simulation. The results illustrating mode hybridization are shown in Fig. 2. We found two hybrid modes (hereafter referred to as Hyb_1 and Hyb_2) between TE_0 and TM_1 around the waveguide width of w=1.09 μm (Fig. 2(a)), and the mode profiles of Hyb_1 and Hyb_2 are visualized in Figs. 2(b)–2(d) and 2(e)-2(g), respectively. The intensity profiles of these two modes are almost identical, and their corresponding x(horizontal)- and y(vertical)- components of the electric field display the profile of TE_0 and TM_1, respectively. To evaluate the degree of hybridization, we define the TE polarization fraction as follows:

$$\text{TE polarization fraction} = \frac{\int |E_x|^2 dx dy}{\int (|E_x|^2 + |E_y|^2) dx dy}. \tag{1}$$

This parameter characterizes the fraction of transverse field power that is TE polarized. The corresponding TE polarization fractions of the modes Hyb_1 and Hyb_2 in Figs. 2(b) and 2(d) are
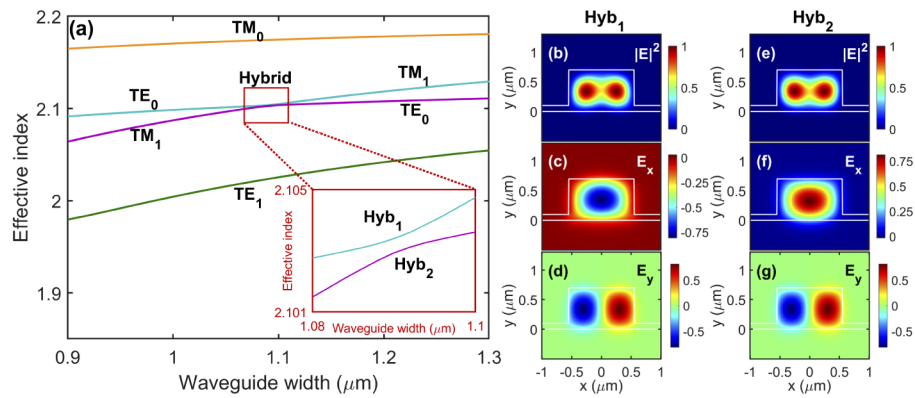
Fig. 2. Waveguide modes without index perturbation. (a) The effective index as a function of the waveguide width for the considered modes at the wavelength of 775 nm. Inset: enlarged view of the hybrid region. (b)-(d): Mode profiles of Hyb_1. (e)-(g): Mode profiles of Hyb_2. (b) and (e) show the intensity distribution; (c), (d), (f) and (g) represent the electric field.
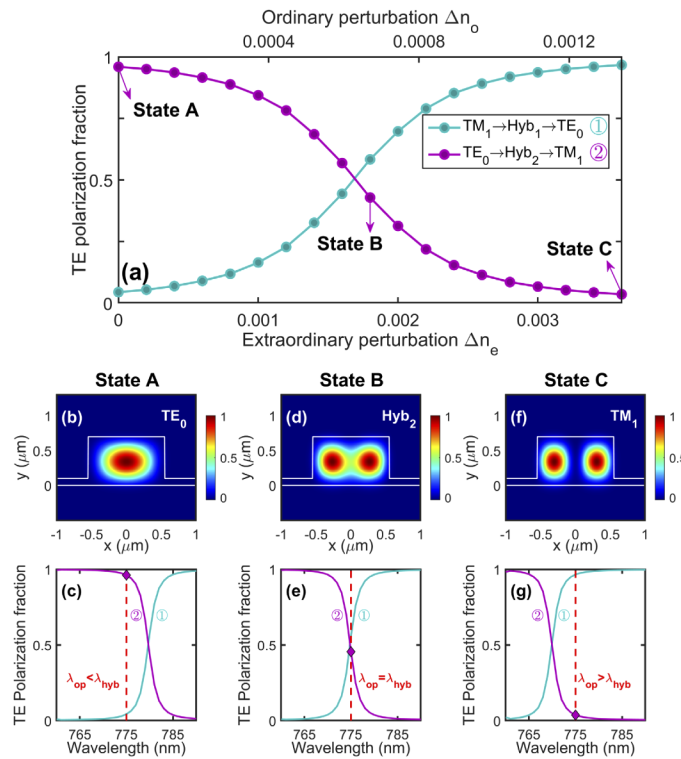

Fig. 3. Mode switching with varying index perturbation. (a) The evolution of modes around hybridization region with varying index perturbation at 775 nm. Bottom and top axes correspond to the perturbation in extraordinary and ordinary indices induced by the same modulating field strength. The intensity profiles of the states A (TE_0), B (Hyb_2) and C (TM_1) indicated in (a) are shown in (b), (d) and (f), and the corresponding polarization states with respect to the wavelength are shown in (c), (e) and (g), respectively. λ_{op} indicates the operation wavelength (775 nm). λ_{hyb} represents the mode hybridization wavelength that shifts from 780 nm (state A) to 770 nm (state C) with varying index perturbation.

calculated to be both around 50%, i.e., the two modes are maximally hybridized between TE and TM at w=1.09 µm, with their powers composed of equal parts of TE and TM components. Given the almost identical field and polarization composition of the two hybrid modes, their effective indices closely coincide while avoid crossing, as manifested in the inset of Fig. 2(a). This anti-crossing behavior distinguishes hybrid modes from an accidental intersection of two orthogonally polarized modes, in which case the two effective index curves can directly cross each other and form a genuine degenerate point [25]. Therefore, these anti-crossings can be used to identify hybrid regions in parameter sweeps. It is worth noting that mode hybridizations only occur between an even-order TE mode and an odd-order TM mode, or vice versa, if the hybridization is induced by broken vertical symmetry, as is the case for ridge waveguides [21].

To obtain mode conversion, we choose the waveguide width to be w=1.1 µm. This sets the operating point in the vicinity of the maximally hybridized condition (w=1.09 µm), while the considered mode is still TE (see state A in Fig. 3(a)). The hybridization can be induced by external electro-optic perturbation, and hence mode conversion is realized by shifting the hybridization condition with the driving voltage.

3. Performance simulation

We demonstrate a polarization mode converter by modulating the mode hybridization behavior using external electro-optic perturbation of the index profile. We show that with the strong electro-optic effect in lithium niobate, the wavelength at which mode hybridization occurs can be actively controlled. This allows for mode conversion without tapering or quasi-phase matching.

3.1. Modulation of mode hybridization

First, we analyze the variation of the mode hybridization behavior when the refractive index is perturbed by a modulating electric field coinciding with the optical axis of lithium niobate (see coordinates in Fig. 1). This configuration engages r_{33}, the largest electro-optic coefficient in lithium niobate. The external field $E_{x(\text{ext})}$ would induce a change in the extraordinary refractive index,

$$\Delta n_{\text{e}} = -\frac{n_e^3}{2} r_{33} E_{x(\text{ext})}. \tag{2}$$

However, with the presence of another non-zero component r_{13} in the electro-optic coefficient tensor of lithium niobate, the ordinary index is also perturbed by

$$\Delta n_{\text{o}} = -\frac{n_o^3}{2} r_{13} E_{x(\text{ext})}. \tag{3}$$

We used the experimental values for r_{33} and r_{13} reported in [26]. The change in the ordinary index is noticeably weaker than that in the extraordinary index by a constant ratio of Δn_{o}=0.3722Δn_{e} at the designed wavelength. When both indices are perturbed simultaneously, the modes switch between TE_0 and TM_1 via the two hybrid modes they form, namely Hyb_1 and Hyb_2 (Fig. 3(a)). For the considered mode conversion, the initial state (state A) is TE_0, as indicated by ~97% TE polarization fraction (see Fig. 3(a)), and by the intensity distribution in Fig. 3(b). Wavelength sweeping under the initial condition (Δn_{o}=Δn_{e}=0) shows that this state is on the edge of the hybrid region, as manifested by Fig. 3(c). The hybrid region spans a spectral range of ~10 nm, within which the polarization state varies rapidly. This confirms high sensitivity to perturbations. As the refractive indices are perturbed, the hybrid wavelength shifts. Consequently, the initial TE_0 mode (state A) at the operation wavelength moves across the hybrid region (state B), and eventually converts to TM_1 mode (state C). The relative positions of these states with respect to the hybrid region are represented in Figs. 3 (c), 3(e) and 3(g), and the corresponding mode profiles are shown in Figs. 3 (b), 3(d) and 3(f). The full dynamic range requires Δn_{e}=0.0036 and Δn_{o}=0.0013, which correspond to an electric field of 22.2 V/µm. The same principle of

operation can be applied to other wavelengths by scaling the waveguide parameters, as long as mode hybridization exists. An inverse conversion from TM_1 to TE_0 (cyan color in Fig. 3(a)) can also be achieved under the same condition.

3.2. Simulation of propagation

It is worth noting that the mode switching described above is considered in a cross section of the waveguide under a static refractive index perturbation. To convert a mode along its propagation, the index perturbation must be implemented longitudinally. Here we demonstrate numerically such a set-up. We consider an electric field profile as shown in Fig. 4(a), and the resultant distributions of extraordinary and ordinary index perturbation are shown in Figs. 4(b) and 4(c), respectively. To realize mode conversion, the perturbed parameter, namely the refractive index here, must be varied slowly. This condition is referred to as "adiabatic", in contrast to a "non-adiabatic" case, where an abrupt change of the perturbed parameter results in insufficient mode conversion [20]. Here we consider an interaction length of 3000 μm, within which the gradient of the electric field, as well as the gradient of the index perturbation, is uniform between z=0 and z=3000 μm. The maximum electric field at z=3000 μm is 22.2 V/μm, corresponding to the field strength required for the final state (state C) in Fig. 3(a). We then inject a TE_0 mode in this waveguide and simulate its propagation using the eigenmode expansion (EME) method [27] (Lumerical EME). The EME propagation results for the proposed device are shown in Figs. 4(d)–4(f). These profiles are taken from a cross-section in the x-z plane at y=350 μm, corresponding to the center height of the waveguide. The intensity distribution changing from TE_0 to TM_1 is observed in 4(d), while 4(e) and 4(f), in conjunction, confirm the energy transfer from the x (or TE) polarized component to the y (or TM) polarized component. The conversion efficiency extracted from the scattering matrix is about 96.8%.
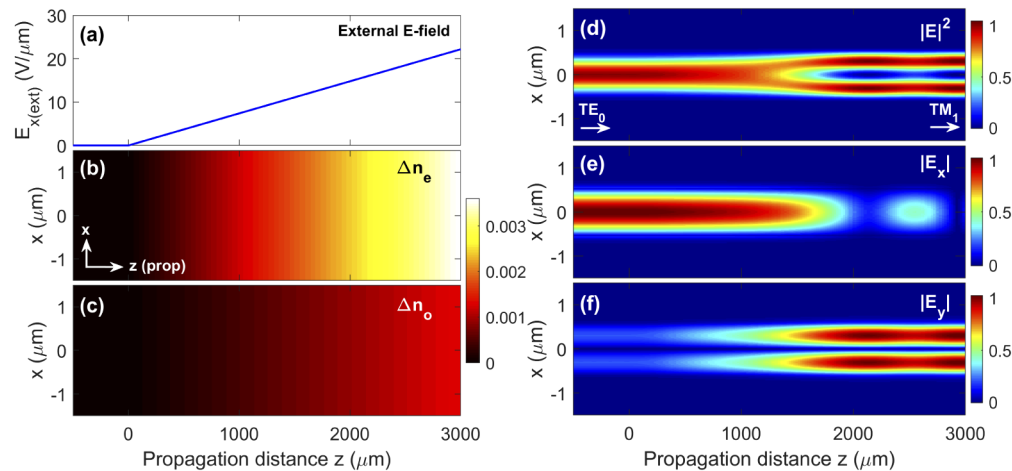

Fig. 4. Simulated polarization mode conversion when a longitudinally varying electric field is applied. (a) The modulating electric field applied in the x direction (or along the optical axis). (b) The extraordinary index perturbation profile. (c) The ordinary index perturbation profile. (d) The intensity profile along propagation. (e) The magnitude profile of the horizontal (TE) component E_x. (f) The magnitude profile of the vertical (TM) component E_y. (d)-(f) correspond to an x-z cross section at y=350 μm.

4. Conclusion

In conclusion, we have numerically demonstrated an actively modulated polarization mode converter in an LNOI ridge waveguide. Our proposed scheme is based on refractive index perturbation and avoids the need for changing the waveguide geometry as required by a tapered approach. It also has the advantage of active modulation. Compared to existing methods which are based on quasi-phase matching, our proposed device does not require periodic poling, thereby greatly simplifying the fabrication process. The realization of a such device paves a new way for application in on-chip signal processing and external field sensing.

Disclosures. The authors declare no conflicts of interest.

Data availability. Data underlying the results presented in this paper are not publicly available at this time but may be obtained from the authors upon reasonable request.

References

1. J. L. Jackel, C. E. Rice, and J. J. Veselka, "Proton exchange for high-index waveguides in LiNbO3," Appl. Phys. Lett. **41**(7), 607–608 (1982).
2. R. V. Schmidt and I. P. Kaminow, "Metal-diffused optical waveguides in LiNbO3," Appl. Phys. Lett. **25**(8), 458–460 (1974).
3. A. Gerthoffer, C. Guyot, W. Qiu, A. Ndao, M. P. Bernal, and N. Courjal, "Strong reduction of propagation losses in LiNbO3 ridge waveguides," Opt. Mater. **38**, 37–41 (2014).
4. H. Hu, R. Ricken, and W. Sohler, "Strong reduction of propagation losses in LiNbO3 ridge waveguides," Opt. Express **17**(26), 24261–24268 (2009).
5. G. Ulliac, V. Calero, A. Ndao, F. I. Baida, and M. P. Bernal, "Argon plasma inductively coupled plasma reactive ion etching study for smooth sidewall thin film lithium niobate waveguide application," Opt. Mater. **53**, 1–5 (2016).
6. I. Krasnokutska, J. L. Tambasco, X. Li, and A. Peruzzo, "Ultra-low loss photonic circuits in lithium niobate on insulator," Opt. Express **26**(2), 897–904 (2018).
7. W. Qiu, M. P. Bernal, A. Ndao, C. Guyot, N. M. Hameed, N. Courjal, H. Maillotte, and F. I. Baida, "Analysis of ultra-compact waveguide modes in thin film lithium niobate," Appl. Phys. B **118**(2), 261–267 (2015).
8. R. Wu, M. Wang, J. Xu, J. Qi, W. Chu, Z. Fang, J. Zhang, J. Zhou, L. Qiao, Z. Chai, and J. Lin, "Long low-loss-lithium niobate on insulator waveguides with sub-nanometer surface roughness," Nanomaterials **8**(11), 910 (2018).
9. J. X. Zhou, R. H. Gao, J. Lin, M. Wang, W. Chu, W. B. Li, D. F. Yin, L. Deng, Z. W. Fang, J. H. Zhang, and R. B. Wu, "Electro-optically switchable optical true delay lines of meter-scale lengths fabricated on lithium niobate on insulator using photolithography assisted chemo-mechanical etching," Chin. Phys. Lett. **37**(8), 084201 (2020).
10. A. Guarino, G. Poberaj, D. Rezzonico, R. Degl'Innocenti, and P. Günter, "Electro–optically tunable microring resonators in lithium niobate," Nat. Photonics **1**(7), 407–410 (2007).
11. M. Zhang, C. Wang, R. Cheng, A. Shams-Ansari, and M. Lončar, "Monolithic ultra-high-Q lithium niobate microring resonator," Optica **4**(12), 1536–1537 (2017).
12. C. Wang, M. Zhang, X. Chen, M. Bertrand, A. Shams-Ansari, S. Chandrasekhar, P. Winzer, and M. Lončar, "Integrated lithium niobate electro-optic modulators operating at CMOS-compatible voltages," Nature **562**(7725), 101–104 (2018).
13. R. Wu, J. Lin, M. Wang, Z. Fang, W. Chu, J. Zhang, J. Zhou, and Y. Cheng, "Fabrication of a multifunctional photonic integrated chip on lithium niobate on insulator using femtosecond laser-assisted chemomechanical polish," Opt. Lett. **44**(19), 4698–4701 (2019).
14. M. Mahmoud, L. Cai, C. Bottenfield, and G. Piazza, "Lithium niobate electro-optic racetrack modulator etched in Y-cut LNOI platform," IEEE Photonics J. **10**(1), 1–10 (2018).
15. M. Xu, M. He, H. Zhang, J. Jian, Y. Pan, X. Liu, L. Chen, X. Meng, H. Chen, Z. Li, and X. Xiao, "High-performance coherent optical modulators based on thin-film lithium niobate platform," Nat. Commun. **11**(1), 3911 (2020).
16. T. Ding, Y. Zheng, and X. Chen, "On-chip solc-type polarization control and wavelength filtering utilizing periodically poled lithium niobate on insulator ridge waveguide," J. Lightwave Technol. **37**(4), 1296–1300 (2019).
17. Y. Niu, C. Lin, X. Liu, Y. Chen, X. Hu, Y. Zhang, X. Cai, Y. X. Gong, Z. Xie, and S. Zhu, "Optimizing the efficiency of a periodically poled LNOI waveguide using in situ monitoring of the ferroelectric domains," Appl. Phys. Lett. **116**(10), 101104 (2020).
18. K. Mertens, B. Scholl, and H. J. Schmitt, "New highly efficient polarization converters based on hybrid supermodes," J. Lightwave Technol. **13**(10), 2087–2092 (1995).
19. K. Mertens, B. Opitz, R. Hovel, K. Heime, and H. J. Schmitt, "First realized polarization converter based on hybrid supermodes," IEEE Photonics Technol. Lett. **10**(3), 388–390 (1998).
20. D. Dai, Y. Tang, and J. E. Bowers, "Mode conversion in tapered submicron silicon ridge optical waveguides," Opt. Express **20**(12), 13425–13439 (2012).

21. A. Kaushalram, G. Hegde, and S. Talabattula, "Mode hybridization analysis in thin film lithium niobate strip multimode waveguides," Sci. Rep. **10**(1), 16692 (2020).
22. L. T. Feng, M. Zhang, Z. Y. Zhou, M. Li, X. Xiong, L. Yu, B. S. Shi, G. P. Guo, D. X. Dai, X. F. Ren, and G. C. Guo, "On-chip coherent conversion of photonic quantum entanglement between different degrees of freedom," Nat. Commun. **7**(1), 11985 (2016).
23. K. H. Luo, S. Brauner, C. Eigner, P. R. Sharapova, R. Ricken, T. Meier, H. Herrmann, and C. Silberhorn, "Nonlinear integrated quantum electro-optic circuits," Sci. Adv. **5**, eaat1451 (2019).
24. G. J. Edwards and M. Lawrence, "A temperature-dependent dispersion equation for congruently grown lithium niobate," Opt. Quantum Electron. **16**(4), 373–375 (1984).
25. A. Pan, C. Hu, C. Zeng, and J. Xia, "Fundamental mode hybridization in a thin film lithium niobate ridge waveguide," Opt. Express **27**(24), 35659–35669 (2019).
26. J. A. De Toro, M. D. Serrano, A. G. Cabañes, and J. M. Cabrera, "Accurate interferometric measurement of electro-optic coefficients: application to quasi-stoichiometric LiNbO$_3$," Opt. Commun. **154**(1-3), 23–27 (1998).
27. G. Sztefka and H. P. Nolting, "Bidirectional eigenmode propagation for large refractive index steps," IEEE Photonics Technol. Lett. **5**(5), 554–557 (1993).